

Levy-driven temporally quenched dynamic critical behavior in directed percolation

Yanyang Wang,¹ Yuxiang Yang,^{1,2,*} and Wei Li^{1,2}

¹*Key Laboratory of Quark and Lepton Physics (MOE) and Institute of Particle Physics,
Central China Normal University, Wuhan 430079, China*

²*ESIEA, Campus Ivry sur Seine, 73 bis Avenue Maurice Thorez, 94200 Ivry sur Seine.*

Quenched disorder in absorbing phase transitions can disrupt the structure and symmetry of reaction-diffusion processes, affecting their phase transition characteristics and offering a more accurate mapping to real physical systems. In the directed percolation (DP) universality class, time quenching is implemented through the dynamic setting of transition probabilities. We developed a non-uniform distribution time quenching method in the (1+1)-dimensional DP model, where the random quenching follows a Lévy distribution. We use Monte Carlo (MC) simulations to study its phase structure and universality class. The critical point measurements show that this model has a critical region controlling the transition between the absorbing and active states, which changes as the parameter β , influencing the distribution properties varies. Guided by dynamic scaling laws, we measured the continuous variation of critical exponents: particle density decay exponent α , total particle number change exponent θ , and dynamic exponent z . This evidence establishes that the universality class of Lévy-quenched DP systems evolves with distribution properties. The Lévy-distributed quenching mechanism we introduced has broad potential applications in the theory and experiments of various absorbing phase transitions.

I. INTRODUCTION

Classical phase transitions involve both equilibrium and non-equilibrium systems, which are closely related both theoretically and experimentally. Even equilibrium systems in steady states may deviate from equilibrium or undergo relaxation processes due to external disturbances or shocks. The Directed Percolation (DP) model, similar to the Ising model in equilibrium phase transitions, is considered a key representative of non-equilibrium phase transitions and has been extensively studied. Several theoretical methods, including mean-field theory, density matrix renormalization, low-density series expansions, and low-order field theory approximations, applied to the Ising model, have also been used to study non-equilibrium systems[1–4]. Moreover, Monte Carlo (MC) simulations have been adapted for non-equilibrium reaction-diffusion systems and have evolved into widely established simulation techniques[5–7].

The Directed Percolation (DP) model, with its robust stability, introduced the concept of universality classes. According to Janssen and Grassberger’s conjectures[8–10], systems transitioning from an absorbing state to an active state under specific conditions belong to this universality class. Representative models include, but are not limited to, interface growth[11], contact processes[12], and turbulence[13]. The evolution of reaction-diffusion systems, when determining the DP universality class, typically relies on fixed transition probabilities that maintain the spatial and temporal stability of conservation laws[14]. However, real-world physical systems often deviate from the DP model[15–17]. For example, material inhomogeneity, the impact of climate

change on epidemics, and the randomness in biological migration introduce complexities that disturb transition probabilities in absorbing phase systems. Systems that incorporate dynamic changes in transition probabilities, known as quenched disorder DP systems, may provide a more accurate representation of real-world systems with complex environmental conditions.

For time quenching in the DP system, quenched disorder can be introduced by altering the conditional probabilities at each time step. Consider the Langevin equation of the DP model[18, 19].

$$\partial_t \varrho(t, \mathbf{r}) = \tau \varrho(t, \mathbf{r}) - g \varrho(t, \mathbf{r})^2 + D \nabla^2 \varrho(t, \mathbf{r}) + \eta(t, \mathbf{r}) \quad (1)$$

The equation describes the time evolution of particle density in the DP system at a coarse-grained level, accounting for fluctuation. The parameter g controls the particle annihilation rate, while D represents the diffusion constant. The parameter τ combines particle branching and annihilation, determining whether the system exhibits percolation. Time quenching disorder is introduced by adding noise to τ [20].

$$\tau \rightarrow \tau + \chi(t). \quad (2)$$

Adding disorder noise undermines the robustness of the DP universality class, altering its critical properties[21]. For example, Jensen showed through low-density series expansion that multiple critical exponents change continuously with varying disorder strength[22] and tested two simple forms of disorder, where the conditional probability p at each time step is determined by a random number r_t and the parameter α_1 [23]. p can either be a fixed value or a random number within the range $[p - \alpha_1, p + \alpha_1]$. Monte Carlo simulations were used to measure the system’s critical exponents, revealing that they change with disorder strength. This indicates that the introduction of time quenching disorder modifies the symmetry and

* yuxyang@mails.ccn.u.edu.cn

conservation laws of the DP system, leading to a change in its universality class.

Introducing different forms of disorder may cause the system to belong to different universality classes, enabling the exploration of how the universality class changes with various quenched disorder forms. Most of the aforementioned quenched structures are stable and follow a uniform distribution within a specific range. In real biological and physical systems, however, the quenched disorder with specific non-uniform distributions may more accurately describe the system's evolution over time. The characteristic distribution of quenched disorder significantly influences changes in the system's conditional probabilities. The concept of Lévy flights has attracted widespread attention in fields such as epidemiology, complex systems, and biodynamics[24]. Due to its property of short-range, long-distance expansion, Lévy flights are increasingly applied in scenarios such as incubation periods and memory effects[25]. We introduce a quenched form with a symmetric Lévy distribution into the (1+1)-dimensional DP system and observe the changes in the system's critical point and exponents. We also explore how the system's universality class changes before and after the introduction of quenched disorder. Considering the long-term evolution of the DP system, when quenched disorder becomes non-uniform and more random, the DP model shows broader applications in diverse physical scenarios. The following sections provide a detailed introduction to the symmetric Lévy distribution time-quenching DP model and its dynamic evolution.

The structure of our paper is as follows: In Sec.II, we introduce the standard DP model and the method for incorporating distributed time quenching. Sec.III provides a brief overview of the dynamic scaling laws of absorbing phase transitions, which serve as the theoretical basis for the Monte Carlo simulations in this model. Our experimental results and analysis are presented in Sec.IV, where Sec.IV.A shows a preliminary analysis of the phase diagram of the model's cluster graph. Sec.IV.B provides a detailed explanation of the critical point determination process. In Sec.II.C, we measure the critical exponents α, θ , and z . Finally, Sec.V concludes the paper with a summary of our findings.

II. MODEL

A real-world example of directed percolation is water flow through porous rocks in geology. Unlike isotropic percolation problems[26], directed percolation is driven by a force field in a particular direction. This could correspond to water flow under the influence of gravity or the dynamic distribution of spin alignments in the presence of an external magnetic field. In non-equilibrium statistical mechanics, DP is a stochastic multi-particle process. Under strict causality, DP is a long-term non-equilibrium system initiating a reaction-diffusion process, which includes:

- $A \rightarrow \emptyset$ particle removal
- $A \rightarrow 2A$ offspring production
- $2A \rightarrow A$ coalescence
- $A \rightarrow A$ single-particle diffusion

In this model, ' A ' represents active particles, and ' \emptyset ' represents inactive particles. For a square lattice model, the evolution of the DP system starting from a single seed is shown in Fig. 1. The occupation state of site s_i at the next time step is determined by the following update rule[2, 27, 28].

$$s_{i,t+1} = \begin{cases} 1 & \text{if } s_{i-1,t} \neq s_{i+1,t} \text{ and } z_i(t) < p, \\ 1 & \text{if } s_{i-1,t} = s_{i+1,t} = 1 \text{ and } z_i(t) < p(2-p), \\ 0 & \text{otherwise,} \end{cases} \quad (3)$$

where z_i is a random number between $[0, 1]$, and p is the conditional probability that governs the system's evolution. The value $s_{i,t+1}$ at the next time step represents the occupation state of site i , with 1 indicating an active site and 0 indicating an empty site. The state update of a site depends on the connection states of its neighboring edges[2], and this rule defines the DP model, also known as bond DP. In the ordinary DP process, the conditional probability p is usually fixed. However, external noise and variations in unstable fields cause the interaction strength to vary dynamically over time. For time-dependent quenched disorder in the DP system, the conditional probability p can be modified as follows:

$$p \rightarrow p + \delta(t). \quad (4)$$

$\delta(t)$ represents the increment of the conditional probability at each time step during the DP evolution. As previously stated, we aim to introduce a more complex time-quenching method to analyze DP-like behavior in real physical systems. This quenching is non-uniform and follows a particular distribution like $\delta(t) = P(z)$, where $P(z)$ represents the probability density function (PDF) of the random variable z . We have employed the stable symmetric Lévy distribution, known for its heavy-tailed characteristic, and commonly used to describe short-time, long-range expansion processes in biological systems[29], economics[30], and high-energy astrophysical phenomena[31]. To study the impact of Lévy-distributed random processes on DP dynamics with time quenching, we specify the method for generating random step sizes and calculating the corresponding probability density function.

At each time step, we generate random step sizes following the Lévy distribution and use numerical integration to obtain the corresponding PDF. This is then used as the quenching factor for the conditional probability in the DP process. The method for generating random step sizes with a stable symmetric Lévy distribution has been precisely determined within a range[32].

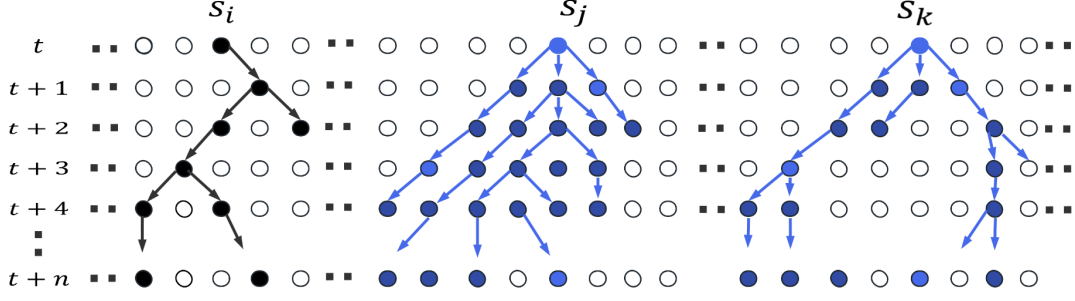


FIG. 1. The evolution of the time-quenching DP system, compared to the ordinary DP process, is illustrated with examples. Here, S_i represents the evolution of the ordinary DP process, S_j represents the long-duration, high-percolation local multi-particle structures that may arise under time quenching, and S_k represents another possible effect, where large vacancy gaps appear under low transition probabilities.

$$L_\beta(z) = \frac{1}{\pi} \int_0^\infty \exp(-q^\beta) \cos(qz) dq, \quad (5)$$

where β plays a key role in determining the properties of the distribution, particularly its scaling behavior, and acts as the characteristic exponent that governs the large-scale power-law behavior. The algorithm process for generating random step lengths s that satisfy this distribution is as follows[32]:

$$s = \frac{u}{|v|^{1/\beta}}, \quad (6)$$

where u, v follow normal distribution

$$u \sim N(0, \sigma_u^2), \quad v \sim N(0, \sigma_v^2). \quad (7)$$

Additionally,

$$\sigma_u = \left\{ \frac{\Gamma(\beta+1) \sin(\pi\beta/2)}{\Gamma[(\beta+1)/2] \beta 2^{(\beta-1)/2}} \right\}^{1/\beta}, \quad \sigma_v = 1. \quad (8)$$

The random step size s results from the combination of two independent random variables, u and v , each following a normal distribution. The algorithm yields high accuracy for β values within the range (0.75, 1.95). The probability density function is computed using the Fast Fourier Transform (FFT) technique. However, for $\beta \leq 1$, the maximum likelihood estimation may fail to converge[33]. Unless otherwise specified, we use β values greater than 1 to minimize the systematic errors introduced by the numerical simulation. When $\beta \in (1.0, 1.95)$, the random step lengths generated by the above algorithms result in a PDF $P(z)$ that is highly consistent with distribution (5). We anticipate that the DP evolution structure will exhibit changes under the influence of this complex quenching factor, as illustrated in Figure 1. Over an extended time period, no particles may survive, or particles may continue to branch and diffuse in a specific direction with a high transition probability.

The introduction of this complex time-quenching factor into a standard DP system will undoubtedly alter the dynamics of the DP system. Through Monte Carlo simulations, we analyze the critical points and exponents of this distributed quenching DP system to investigate changes in its universality class and potential applications in complex physical systems. The following sections present the scaling relations for absorbing phase transition systems and the corresponding Monte Carlo methods used for analysis.

III. DYNAMIC SCALING LAWS IN ABSORBING PHASE TRANSITIONS

In equilibrium statistical mechanics, second-order phase transitions are typically associated with the divergence of the order parameter, such as the magnetic susceptibility of the 2D Ising model, which diverges near the critical point[1]. Absorbing phase transitions, like those in equilibrium statistical physics, exhibit scaling law characteristics that can be analyzed using scaling functions. Near the critical point of an absorbing phase transition model, the correlation length typically satisfies:

$$\xi \sim |P - P_c|^{-\nu}, \quad (9)$$

where P is the control parameter governing the phase transition, and P_c represents the critical value of this control parameter, such as the percolation probability in the DP model. The exponent ν characterizes the divergence of the correlation length at the critical point. Unlike equilibrium systems, in non-equilibrium systems, time and space correlations must be treated separately due to their independent degrees of freedom. For the dynamics of the DP system, the initial configuration significantly influences the properties and measurements of the order parameter. Similarly, the dynamic scaling laws of absorbing phase transitions are closely linked to the initial conditions.

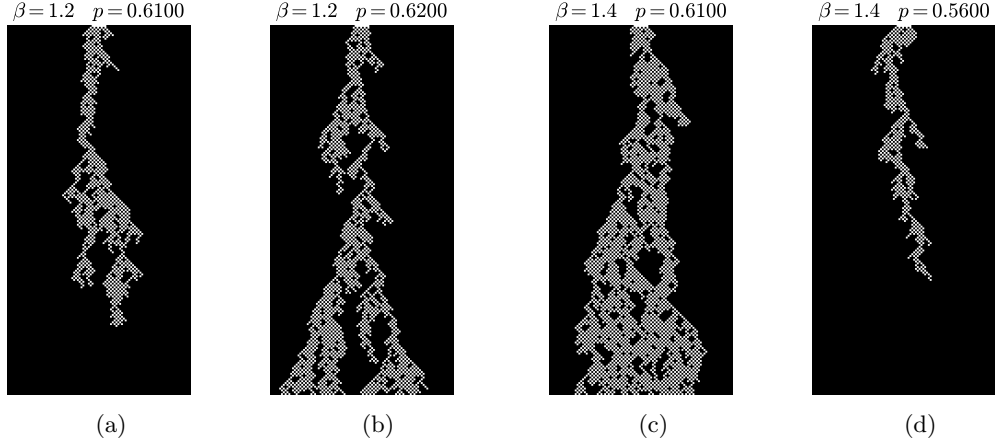


FIG. 2. Cluster diagrams of the Lévy-distributed time-quenching DP system are shown. (a) and (b) illustrate that, for the same β value but different conditional probabilities p , the cluster diagrams exhibit a transition from the absorbing state to the active state, along with the appearance of large vacancy gaps and edge "avalanche" phenomena. (c) and (d) illustrates the phase transition behavior as the conditional probability changes, with different control parameters than those in (a) and (b). These phenomena indicate that the phase transition characteristics of the time-quenching DP system are influenced by the properties of the Lévy distribution.

Under the homogeneous initial condition, at the critical point, the time evolution of the particle density at active sites is described by

$$\rho(t) = \left\langle \frac{1}{N} \sum_i s_i(t) \right\rangle \quad (10)$$

where $s_i(t)$ represents the position of active particles at time t , and N is the total number of sites in the system. For an infinite system size, $\rho(t)$ follows the scaling form:

$$\varrho(t) \simeq \lambda^{-\beta} \tilde{R}_f(\lambda^{-\nu_{\parallel}} a_t t). \quad (11)$$

where $t \rightarrow \lambda^{-\nu_{\parallel}} t$ represents the scaling of time t with the time correlation length $\xi \sim |\tau|^{-\nu_{\parallel}}$ represents the active sites with fully occupied initial conditions. By integrating the scaling form of $\rho(t)$ and setting $\lambda^{-\nu_{\parallel}} a_t t = 1$, we obtain the dynamic scaling law with the critical exponent α :

$$\rho(t) \sim t^{-\alpha}. \quad (12)$$

Based on this dynamic scaling relation, for an absorbing phase transition system away from the critical point, the time evolution of particle density will deviate from a power-law decay. Therefore, this scaling law can be used as a criterion for determining the system's critical position, and under homogeneous initial conditions, random errors are significantly reduced.

In addition to simulating the reaction-diffusion process under the homogeneous initial condition, evolving clusters from locally active seeds can also simulate the absorbing phase transition and measure critical exponents[2]. Under single-particle active conditions,

when the control parameter $\tau > 0$, the system exhibits an active state with particle survival, whereas for $\tau < 0$, it is in an absorbing state with finite clusters. When the system is at the critical point, the time evolution of the characteristic quantities $\langle N(t) \rangle$ and $\langle R^2(t) \rangle$ follows:

$$\langle N(t) \rangle \sim t^{\theta}, \quad \langle R^2(t) \rangle \sim t^{\frac{z}{2}}. \quad (13)$$

where $\langle N(t) \rangle$ is the average number of active particles in all clusters at time t , and $\langle R^2(t) \rangle$ is the mean square displacement of all active particles t from the initial active seed s_0 , known as the mean squared spreading. The critical exponents θ and z are referred to as the initial slip exponent and the expansion exponent, respectively. The measured values of the critical exponents α , θ , and z are crucial for determining the universality class. Within the same universality class, these critical exponents typically do not change significantly.

IV. RESULT

A. Analysis of phase diagram features

Under the influence of spatially quenched disorder, the DP system still undergoes a phase transition from the absorbing state to the active state[14, 34, 35]. However, it remains to be verified whether time quenching with a specific distribution preserves the general characteristics of the absorbing phase transition. To investigate this, we first obtained partial cluster graphs for a finite-sized system over a specific evolution time. As shown in Fig. 2(a) and (b), we chose a Lévy distribution with the control parameter $\beta = 1.2$. When the probability is small, the system eventually reaches the absorbing state after

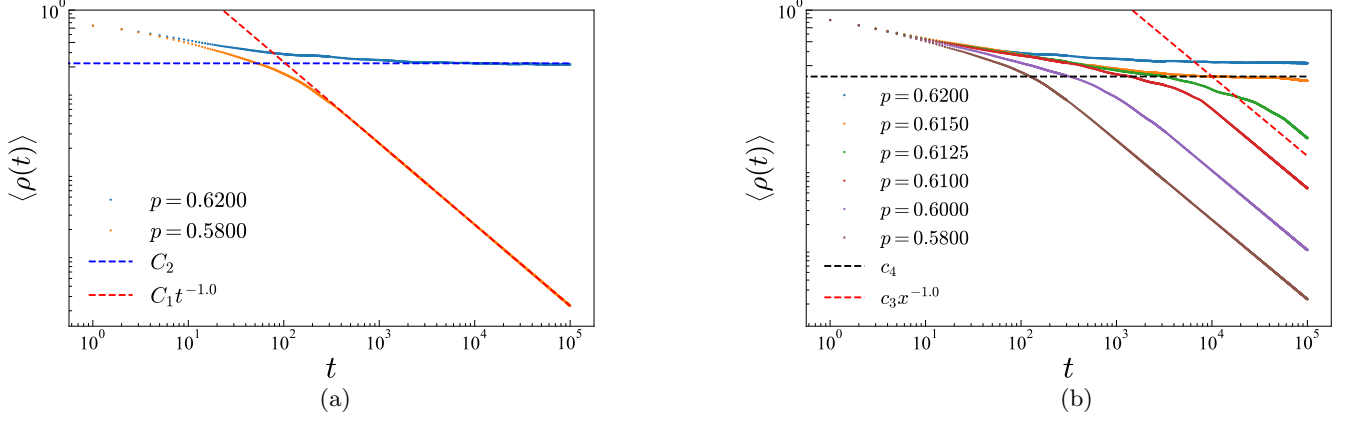


FIG. 3. (a) Preliminary measurement of the critical region in the Lévy-distributed time-quenching DP model for $\beta = 1.2$. The red line represents the system in the absorbing state after a long-time evolution, and the blue curve indicates the system in the active state. (b) Using the auxiliary lines y_1 and y_2 for discrimination, the critical region is gradually narrowed with the bisection method. At the boundary of the interval $[0.6125, 0.6150]$, the system exhibits characteristics of both the absorbing and active states.

sufficient time evolution. When the probability is large, the cluster graph shows the active state, with particles surviving for an extended period. This suggests that under time quenching with a specific distribution, the DP system retains the characteristics of the absorbing phase transition. Additionally, we observed large gaps in the vacancy regions of the cluster centers, possibly caused by the quenched disorder from the heavy-tailed distribution, where particles remain in a low-excitation state for an extended period. Correspondingly, quenching may also lead to edge "avalanche" effects. The accumulated high percolation probability can persist, enabling particles to continuously survive in one direction. This phenomenon can occur even in a relatively stable absorbing state, as shown in Fig. 2(a).

When the control parameter β of distributed quenching is varied, the system transitions from the absorbing state to the active state. As shown in Fig. 2(b) and (c), when the transfer probability p is set to 0.6100, the system with $\beta = 1.2$ stays in the absorbing state, while the system with $\beta = 1.4$ transitions to the active state. Furthermore, when the percolation probability is sufficiently small, as shown in Fig. 2(d) where $p = 0.5600$, the system again exhibits the characteristics of the absorbing state. We expect that the value of β will significantly influence the spatiotemporal evolution of the distributed quenching DP system, resulting in different critical points and exponents, and ultimately altering its universality class.

B. Determination of the critical point

The simple analysis of the cluster graph between the absorbing and active states in the previous section provides an initial understanding of the phase characteristics of the DP system under specific distributional time quench-

ing. However, this is not enough to precisely quantify the impact of quenching on the DP system. To address this, we performed extensive simulations under full seed conditions and used periodic boundary conditions to minimize system errors, aiming to accurately determine the critical point.

For $\beta = 1.2$, we first generated two sets of clusters for $p = 0.5800$ and $p = 0.6200$. The system size was 10000, with 10000 time steps, repeated 100 times to obtain valid samples for averaging. Based on the dynamic scaling laws of absorbing phase transitions described in Sec. II, we computed the long-time average particle density $\langle \rho(t) \rangle$, as shown in Fig. 3(a). When $p = 0.5800$, the particle density evolves according to a power law with an exponent of -1 , indicated by the orange data points on the log-log plot. This is because the system is in the absorbing state, and after sufficient time evolution, the particle density $\rho(t)$ follows:

$$y_1 = \langle \rho(t) \rangle = \left\langle \frac{C_0}{lt} \right\rangle = C_1 t^{-1.0}, \quad t > t_0, \quad (14)$$

where for $t > t_0$, no particles survive, and the system stays in the absorbing state. C_0 is the average number of active particles throughout the system's evolution and l is the system's size. When $p = 0.6200$, as shown in Fig. 3(a), the particle density decays more gradually with time and eventually stabilizes at a constant value, deviating from the global power-law characteristic in the critical state. We can use two auxiliary lines, y_1 and y_2 , to help identify whether the system is at the critical point for a given transfer probability p , where $y_2 = C_2$. From Fig. 3(a), for $\beta = 1.2$, we can preliminarily conclude that the critical point lies between 0.5800 and 0.6200, i.e., $P_c \in (0.5800, 0.6200)$.

To refine the determination of the critical point, we applied the bisection method to narrow the range of the transfer probability p . The results for particle density $\rho(t)$ at additional transfer probabilities are shown in Fig. 3(b). At the later stages of the finite-size system's time evolution, the differences in initial transfer probabilities become more pronounced, helping to accurately identify the critical region. After discarding situations where the system reaches the absorbing state after a sufficient number of time steps, we can further narrow the critical point range to $P_c \in (0.6125, 0.6150)$. To reduce errors further, we increased the system's average by using 200 samples of $10^4 \times 10^5$ clusters. At this narrower range of measurements, the results for particle density are shown in Fig. 4. At this point, auxiliary lines no longer assist in pinpointing the precise location of the critical point. We used an alternative method to quantify the results' reliability and accuracy. As shown in Fig. 4, we obtained the fitting goodness for $p = 0.6143, 0.6140, 0.6137$ using power-law fitting, defined as:

$$R^2 = 1 - \frac{\sum (y_a - y_p)^2}{\sum (y_a - y_m)^2}, \quad (15)$$

where y_a is the actual value of the particle density, y_p is the corresponding predicted value of the fitted curve, and y_m is the average of the actual values.

The value of R^2 quantifies the goodness of fit for the power-law decay of the particle density $\rho(t)$. For $p = 0.6143, 0.6140, 0.6137$, the corresponding R^2 values are $R_1^2 = 0.9812(5), R_2^2 = 0.9942(7)$, and $R_3^2 = 0.9836(9)$, indicating that the system exhibits optimal power-law decay of particle density at $p = 0.6140$. Therefore, when $\beta = 1.2$, the critical point of the Lévy-distributed quenching DP system is $P_c = 0.614(0)$, with an error smaller than 0.0003.

Based on the decay of particle density at different transfer probabilities, we confirmed that under Lévy-distributed time quenching, the DP system indeed exhibits a phase transition with a critical point distinguishing the absorbing state. Larger-scale Monte Carlo simulations lead to a more accurate determination of the critical region. As observed from the cluster graph analysis in the previous section, when β takes different values, the system transitions from the absorbing state to the active state. We expect that under the control of the Lévy distribution parameter β , the time-quenching DP system will exhibit changes in the critical point. Therefore, under the same statistical averaging conditions, we measured the critical point for various values of β using the methods described above. The results are summarized in Table I, and Fig. 5 shows an example for $\beta = 1.95$. From Table I, we infer that the critical point of the Lévy-distributed quenching DP system changes continuously with β .

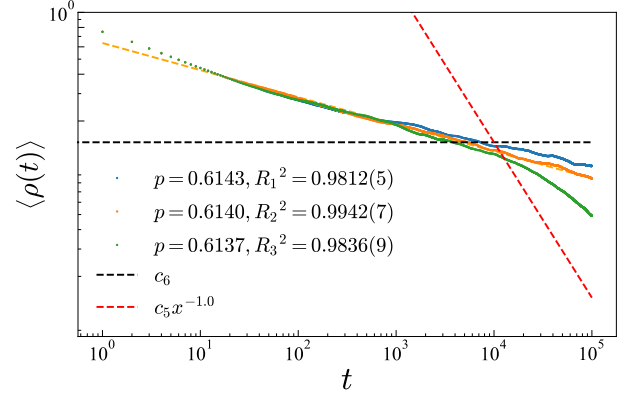


FIG. 4. As the critical region is further narrowed, the critical point is determined using the goodness of fit. The value $p = 0.6140$ corresponds to the optimal goodness of fit, making it a reliable reference for determining the critical point.

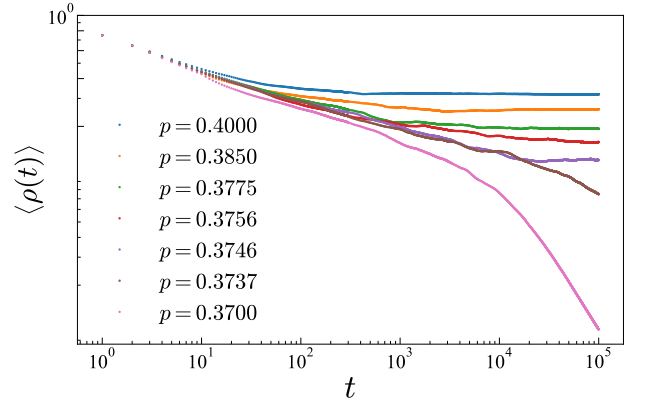


FIG. 5. For $\beta = 1.95$, the statistical average of particle density as a function of time is measured for various percolation probabilities p . In the narrower critical interval $(0.3737, 0.3746)$, the critical point is determined as $P_c = 0.374(1)$.

β	P_c	α	θ	$\frac{2}{z}$
1.2	0.614(0)	0.181(7)	0.315(2)	1.201(0)
1.4	0.566(4)	0.162(1)	0.346(3)	1.182(4)
1.6	0.505(6)	0.152(5)	0.378(0)	1.156(8)
1.8	0.426(9)	0.143(6)	0.396(1)	1.127(6)
1.95	0.374(1)	0.136(6)	0.421(7)	1.081(2)

TABLE I. The determination of the critical point P_c and the measurements of the critical exponents α , θ , and z for different values of the parameter β .

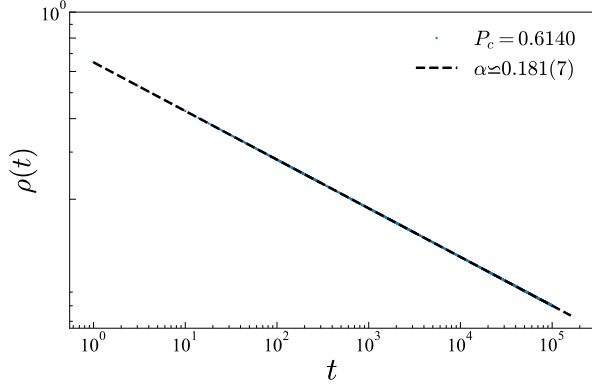


FIG. 6. For $\beta = 1.2$, the critical exponent α is obtained by fitting the particle density decay, as described by equation (16). Using the averaged fitting results from five sets of 200 clusters with system sizes $10^4 \times 10^5$, the critical exponent is found to be $\alpha = 0.181(7)$.

C. Measurement of the critical exponents α, θ and z

Under homogeneous initial condition MC simulations, the time evolution of the particle density at the critical point is described by

$$\rho(t) \sim t^{-\alpha}. \quad (16)$$

We used this power law to accurately determine the critical point for different values of β , as $\rho(t)$ exhibits power-law deviations when the transfer probability p deviates from P_c . To minimize random errors and accurately determine the critical exponent α , we conducted extensive simulations at $\beta = 1.2$ and $p = 0.6140$. As shown in Fig. 6, we generated five sets of 20000 clusters with system sizes of $10^4 \times 10^5$ and repeated the simulations 100 times to average the results. The final measured value of α was stable at $\alpha = 0.181(7)$. The measurements for α at different β values are summarized in Table I.

Unlike the homogeneous initial condition simulation, under one active particle initial conditions, as described in Sec. II, the average total particle number $\langle N(t) \rangle$ and mean squared displacement $\langle R^2(t) \rangle$ follow the equation of (13). To reduce finite-size effects, we fixed the initial active seed at the center of the system and used periodic boundary conditions. The preliminary measurement results for the average particle number are shown in Fig. 7, with a system size of 10^4 , 100,000 time steps, and 2000 samples for averaging. When $\beta = 1.2$ and $p = 0.6140$, the fitted value for θ was 0.313(2). When p deviates from 0.6140, we observe significant power-law deviations. Under the same system settings and statistical averages, we measured the mean square displacement $R^2(t)$ of the initially active seed, and the power law fitting results are shown in Fig. 8. The measured values of θ and $2/z$ for different β values are summarized in Table I.

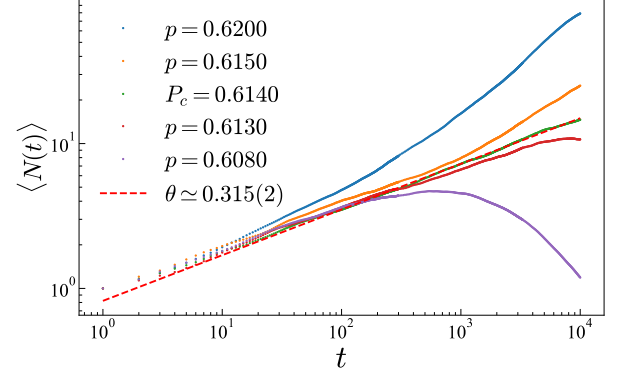


FIG. 7. For $\beta = 1.2$, the variation in the average total number of surviving particles is measured for various percolation probabilities p . The value of the critical exponent θ is determined using the dynamic scaling law (13).

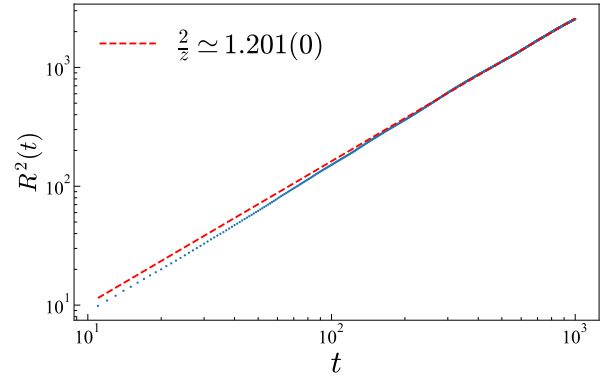


FIG. 8. For $\beta = 1.2$, the value of the critical exponent z is obtained by statistically measuring the mean squared displacement, using the dynamic scaling law (13).

From the critical exponent α measurements in Table I, we observe that as the Lévy distribution parameter β increases, α decreases. This is consistent with the characteristics of the Lévy distribution: as β increases, the kurtosis decreases, and the distribution becomes flatter. This suggests that the quenching of the transfer probability becomes less severe at higher β , causing the particle reaction-diffusion process to proceed more slowly over time, leading to a gradual change in particle density. The observed trend in the variation of the critical exponents with the distributional characteristics supports the physical interpretation. A similar analysis is reflected in the measurements of the critical exponents θ and $2/z$. With sufficient ensemble averaging, power-law fitting yields good results. The measurements of the critical exponents α , θ , and z indicate that under the control of β , the universality class of the Lévy-distributed quenching DP system continuously changes.

V. CONCLUSION

In this paper, we studied the absorbing phase transition behavior of the DP system with Lévy-distributed time quenching. By analyzing the phase diagram and the properties near the critical point, we confirmed the scaling features of the model. Using the dynamic scaling theory of absorbing phase transitions, we determined the critical point location for various values of the distribution parameter β . The critical point results show that, while distributed time quenching alters the critical region of the standard DP system, it preserves the power-law decay characteristic of particle density. We also quantified the critical exponents α , θ , and z . The measured results of these critical exponents are consistent with the critical point and vary with β . Lévy-distributed quenching affects the spatiotemporal symmetry of the DP system, deviating from the DP model and leading to a

new universality class. Unlike uniform quenching, Lévy-distributed quenching, by adjusting parameters such as kurtosis and variance, may provide a more accurate mapping to real physical systems. The analysis of the general characteristics of absorbing phase transitions suggests that distributed spatiotemporal quenching offers a broader theoretical and experimental outlook for more reaction-diffusion processes.

VI. ACKNOWLEDGEMENTS

This work is supported in part by the National Key Research and Development Program of China under Grant No. 2024YFA1611003, the Fundamental Research Funds for Central China Normal University(CCNU24JC007), and the 111 Project, with Grant No. BP0820038. Financially supported by self-determined research funds of CCNU from the college basic research and operation of MOE.

-
- [1] K. Christensen and N. R. Moloney, *Complexity and criticality*, Vol. 1 (World Scientific Publishing Company, 2005).
 - [2] M. Henkel, H. Hinrichsen, S. Lübeck, and M. Pleimling, *Non-equilibrium phase transitions*, Vol. 1 (Springer, 2008).
 - [3] U. C. Täuber, *Critical dynamics: a field theory approach to equilibrium and non-equilibrium scaling behavior* (Cambridge University Press, 2014).
 - [4] D. J. Amit and V. Martin-Mayor, *Field theory, the renormalization group, and critical phenomena: graphs to computers* (World Scientific Publishing Company, 2005).
 - [5] S. Lübeck, Journal of Statistical Mechanics: Theory and Experiment **2006**, P09009 (2006), doi:[10.1088/1742-5468/2006/09/p09009](https://doi.org/10.1088/1742-5468/2006/09/p09009).
 - [6] M. E. Newman and G. T. Barkema, *Monte Carlo methods in statistical physics* (Clarendon Press, 1999).
 - [7] D. Zhong and D. ben Avraham, Physics Letters A **209**, 333 (1995), doi:[10.1016/0375-9601\(95\)00869-1](https://doi.org/10.1016/0375-9601(95)00869-1).
 - [8] P. Grassberger and A. de la Torre, Annals of Physics **122**, 373 (1979), doi:[10.1016/0003-4916\(79\)90109-X](https://doi.org/10.1016/0003-4916(79)90109-X).
 - [9] H.-K. Janssen, Zeitschrift für Physik B Condensed Matter **42**, 151 (1981), doi:[10.1007/BF01319549](https://doi.org/10.1007/BF01319549).
 - [10] P. Grassberger, Zeitschrift für Physik B Condensed Matter **47**, 365 (1982), doi:[10.1007/BF01313803](https://doi.org/10.1007/BF01313803).
 - [11] L.-H. Tang and H. Leschhorn, Physical Review A **45**, R8309 (1992), doi:[10.1103/PhysRevA.45.R8309](https://doi.org/10.1103/PhysRevA.45.R8309).
 - [12] T. E. Harris, The Annals of Probability **2**, 969 (1974), doi:[10.1214/aop/1176996493](https://doi.org/10.1214/aop/1176996493).
 - [13] Y. Pomeau, Physica D: Nonlinear Phenomena **23**, 3 (1986), doi:[10.1016/0167-2789\(86\)90104-1](https://doi.org/10.1016/0167-2789(86)90104-1).
 - [14] H. Hinrichsen, Advances in physics **49**, 815 (2000), doi:[10.1080/00018730050198152](https://doi.org/10.1080/00018730050198152).
 - [15] H. Hinrichsen, A. Jiménez-Dalmaroni, Y. Rozov, and E. Domany, Physical Review Letters **83**, 4999 (1999), doi:[10.1103/PhysRevLett.83.4999](https://doi.org/10.1103/PhysRevLett.83.4999).
 - [16] H. Hinrichsen, A. Jiménez-Dalmaroni, Y. Rozov, and E. Domany, Journal of Statistical Physics **98**, 1149 (2000), doi:[10.1023/A:1018667712578](https://doi.org/10.1023/A:1018667712578).
 - [17] K. A. Takeuchi, M. Kuroda, H. Chaté, and M. Sano, Physical review letters **99**, 234503 (2007), doi:[10.1103/PhysRevLett.99.234503](https://doi.org/10.1103/PhysRevLett.99.234503).
 - [18] R. Cafiero, A. Gabrielli, and M. A. Muñoz, Physical Review E **57**, 5060 (1998), doi:[10.1103/PhysRevE.57.5060](https://doi.org/10.1103/PhysRevE.57.5060).
 - [19] J. Zinn-Justin, *Quantum field theory and critical phenomena*, Vol. 171 (Oxford university press, 2021).
 - [20] H. Janssen, Physical Review E **55**, 6253 (1997), doi:[10.1103/PhysRevE.55.6253](https://doi.org/10.1103/PhysRevE.55.6253).
 - [21] J. Hooyberghs, F. Iglói, and C. Vanderzande, Physical Review E—Statistical, Nonlinear, and Soft Matter Physics **69**, 066140 (2004), doi:[10.1103/PhysRevE.69.066140](https://doi.org/10.1103/PhysRevE.69.066140).
 - [22] I. Jensen, Journal of Physics A General Physics **38** (2005), doi:[10.1088/0305-4470/38/7/003](https://doi.org/10.1088/0305-4470/38/7/003).
 - [23] I. Jensen, Physical review letters **77**, 4988 (1996), doi:[10.1103/PhysRevLett.77.4988](https://doi.org/10.1103/PhysRevLett.77.4988).
 - [24] H. Hinrichsen and M. Howard, The European Physical Journal B-Condensed Matter and Complex Systems **7**, 635 (1999), doi:[10.1007/s100510050656](https://doi.org/10.1007/s100510050656).
 - [25] H. Hinrichsen, Journal of Statistical Mechanics: Theory and Experiment **2007**, P07006 (2007), doi:[10.1088/1742-5468/2007/07/P07006](https://doi.org/10.1088/1742-5468/2007/07/P07006).
 - [26] R. B. Potts, in *Mathematical proceedings of the cambridge philosophical society*, Vol. 48 (Cambridge University Press, 1952) pp. 106–109, doi:[10.1017/S0305004100027419](https://doi.org/10.1017/S0305004100027419).
 - [27] E. Domany and W. Kinzel, Physical Review Letters **53**, 311 (1984), doi:[10.1103/PhysRevLett.53.311](https://doi.org/10.1103/PhysRevLett.53.311).
 - [28] W. Kinzel, Zeitschrift Für Physik B Condensed Matter **58**, 229 (1985), doi:[10.1007/BF01309255](https://doi.org/10.1007/BF01309255).
 - [29] T. Whitney, T. Solomon, and K. Mitchell, “A general approach to the statistics of microbial orientation: Lévy walks, noise, and deterministic motion,” (2025),

- arXiv:2502.13304 [physics.bio-ph].
- [30] Y. Huang, C. Liu, and X. Zhou, “Lévy score function and score-based particle algorithm for nonlinear lévy–fokker–planck equations,” (2024), arXiv:2412.19520 [math.NA].
 - [31] S. Aerdker, L. Merten, F. Effenberger, H. Fichtner, and J. B. Tjüs, *Astronomy & Astrophysics* **693**, A15 (2025).
 - [32] R. N. Mantegna, *Physical Review E* **49**, 4677 (1994), doi:10.1103/physreve.49.4677.
 - [33] L. Wang and J.-H. Zhang, in *The Second International Symposium on Optimization and Systems Biology, Li-jiang, China* (2008) pp. 381–388.
 - [34] T. Vojta, *Physical Review E—Statistical, Nonlinear, and Soft Matter Physics* **70**, 026108 (2004), doi:10.1103/PhysRevE.70.026108.
 - [35] T. Vojta and M. Dickison, *Physical Review E—Statistical, Nonlinear, and Soft Matter Physics* **72**, 036126 (2005), doi:10.1103/PhysRevE.72.036126.
 - [36] X.-S. Yang, *Nature-inspired metaheuristic algorithms* (Luniver press, 2010).